Loftie-Eaton, W. et al. (2013). Balancing redox cofactor generation and ATP synthesis : key microaerobic responses in thermophilic fermentations.
Biotechnology and Bioengineering, 110(4): 1057 – 1065
http://dx.doi.org/10.1002/bit.24774

Balancing redox cofactor generation and ATP synthesis: key microaerobic responses in thermophilic fermentations

Wesley Loftie-Eaton, Mark Taylor, Kerry Horne, Marla I. Tuffin, Stephanie G. Burton and Don A. Cowan

Abstract

Geobacillus thermoglucosidasius is a Grampositive, thermophilic bacterium capable of ethanologenic fermentation of both C5 and C6 sugars and may have possible use for commercial bioethanol production [Tang et al., 2009; Taylor et al. (2009) Trends Biotechnol 27(7): 398–405]. Little is known about the physiological changes that accompany a switch from aerobic (high redox) to microaerobic/fermentative (low redox) conditions in thermophilic organisms. The changes in the central metabolic pathways in response to a switch in redox potential were analyzed using quantitative real-time PCR and proteomics. During low redox (fermentative) states, results indicated that glycolysis was uniformly up-regulated, the Krebs (tricarboxylic acid or TCA) cycle non-uniformly downregulated and that there was little to no change in the pentose phosphate pathway. Acetate accumulation was accounted for by strong down-regulation of the acetate CoA ligase gene (acs) in addition to up-regulation of the pta and ackA genes (involved in acetate production), thus conserving ATP while reducing flux through the TCA cycle. Substitution of an NADH dehydrogenase (down-regulated) by an up-regulated NADH:FAD oxidoreductase and upregulation of an ATP synthase subunit, alongside the observed shifts in the TCA cycle, suggested that an oxygenscavenging electron transport chain likely remained active during low redox conditions. Together with the observed up-regulation of a glyoxalase and down-regulation of superoxide dismutase, thought to provide protection against the accumulation of toxic phosphorylated glycolytic intermediates and reactive oxygen species, respectively, the changes observed in G. thermoglucosidasius NCIMB 11955 under conditions of aerobic-to-microaerobic switching were consistent with responses to low pO2 stress.

Introduction

Commercial production of ethanol for use as a fuel additive relies principally on the fermentation of starch or sucrose derived glucose by Saccharomyces cerevisiae (Hahn-Hagerdal et al., 2006). An understandable objection to the large scale production of ethanol via such methods is that the fermentative substrates generally originate from foodstuffs such as maize and sugarcane. The use of alternative non-food grade carbon feedstocks, principally lignocellulose, has received considerable attention over the last decade. It is now widely recognized that for efficient ethanol production from lignocellulosic feedstocks via

fermentation, the production organism must possess the ability to catabolize both hexose and pentose monomers. Ideally such an organism should have the capacity to degrade polymeric saccharides in a combined hydrolysis and continuous fermentation process (Taylor et al., 2009).

Several approaches have been adopted to address these issues, including improving the catabolic functionality of known ethanologens such as S. cerevisiae (Matsushika et al., 2009; Patnaik, 2008) and Zymomonas (Panesar et al., 2006; Rogers et al., 2007) and engineering the fermentation pathways of catabolically versatile host strains such as Escherichia coli (Clomburg and Gonzalez, 2010; Wang et al., 2008; Zhou et al., 2008). Recent and novel approaches exploit the natural catabolic promiscuity of thermophilic bacteria (Cripps et al., 2009; Shaw et al., 2008; Tang et al., 2009; Taylor et al., 2009).

One such example is the genetic engineering of a near homo-ethanologenic variant of G. thermoglucosidasius (Cripps et al., 2009). The fermentative metabolism of this species is poorly understood, as are the physiological changes that accompany shifts in oxygen availability. Only recently have the functional metabolic networks directly involved in organic acid and ethanol production been rigorously investigated (Tang et al., 2009). Using a combination of flux analysis and genome data (NCBI accession number CP002835), the glycolytic, pentose phosphate and TCA pathways were demonstrated to show anaplerotic reactions such as the glyoxylate shunt (Tang et al., 2009).

Microaerobic growth of G. thermoglucosidasius generally resulted in the production of lactate, ethanol, acetate, and formate via lactate dehydrogenase (ldh), acetaldehyde/ alcohol dehydrogenase (acdh/adh), phosphotransacetylase/ acetate kinase (pat/ack) and pyruvate formate lyase (pfl) (Tang et al., 2009). Deletions of some of these genes have been used to confirm functionality and to redirect carbon flux to ethanol production (Cripps et al., 2009). Despite the importance of low redox conditions in the maintenance of ethanologenesis, little is known of the global metabolic adaptations to microaerobic growth or the regulation of specific pathways and networks under such conditions. In order to understand microaerobic physiology in a wider context, a comparative proteomic and targeted gene expression approach was adopted to compare low redox potential or microaerobic growth profiles to suitable (aerobic; high redox) controls.

Materials and Methods

Bacterial Strains, Maintenance, and Growth

G. thermoglucosidasius NCIMB 11955 was obtained from TMO Renewables, Surrey, UK and cultured in media (2TY, TGP, and ASYE) as reported recently in Cripps et al. (2009). Glycerol stocks were plated onto 2TY agar and grown overnight at 608C. Single colonies were subsequently used to inoculate 100 mL pre-warmed TGP contained within a 250 mL conical flask and grown at 658C and 250 rpm until an OD_{600} of approximately 2 had been achieved. The entire 100 mL culture served as an inoculum for continuous cultures grown on ASYE.

Continuous Culture

Experiments were conducted in a 6 L glass BioFlo 3000 fermentor (New Brunswick, Scientific, Edison, NJ) at a working volume of 2.3 L, filled from a stirred 10 L reservoir of ASYE media. The pH was controlled with 1 N NaOH, and agitation and temperature were controlled to the set points as defined by the user. Fermentations were run at 608C, 600 rpm with airflow 1 vvm (control) and 300 rpm with airflow 0.2 vvm (low redox potential or "microaerobic") at pH 6.7. Redox measurements were made in situ with a Broadley-James redox electrode (Broadley-James, Irvine, CA). After inoculation, batch growth proceeded to an optical density (600 nm) of approximately 5 before the culture was switched to continuous culture at a dilution rate of 0.05 h^{-1}. For each aerobic and microaerobic fermentation, steady state was established only after a total of three volume changes, where fluctuation in the optical density was <5% over an 8 h period. Samples (20 mL) were removed at intervals and cells recovered by centrifugation at 13,000 rpm for 5 min. Washed cell pellets (1 mL culture) for proteomic analysis were frozen at -208C until required. Cell pellets (1.5 mL culture) for RNA extraction were resuspended in 0.75 mL RNAlater (Sigma-Aldrich, St. Louis, MO) and stored on ice. The supernatant was retained for HPLC analysis.

HPLC Analysis

Metabolites were analyzed by HPLC on a Rezex RHM monosaccharide column (00H 0132 KO) at 408C with a 10 mM H_2SO_4 mobile phase at a flow rate of 0.6 mL/min. Samples (10 mL) were injected by autosampler and the components detected using either a refractive index detector or at 210 nm on a UV/Vis detector. Concentrations of broth components were determined by comparison to known standards.

Reverse Transcription-PCR (RT-PCR)

Eight 1.5 mL aliquots of bacterial cells were harvested at each of the high and low redox steady states and were immediately resuspended in RNAlater for RNA extraction and purification. RNAlater solution was removed from cell suspensions within 60 min of harvesting by three successive rounds of centrifugation at 4,000 rpm and 48C for 10 min with subsequent resuspension by vigorous vortexing in 1 mL phosphate buffered saline solution (PBS consisting of 8 gL^{-1} NaCl, 0.2 gL^{-1} KCl, 1.44 gL^{-1} Na_2HPO_4, and 0.24 gL^{1} KH_2PO_4 at pH 7.4). RNA was extracted using a Ambion[1] RboPure Bacteria RNA isolation kit (Life Technologies, Carlsbad, CA) as per manufacturer's protocol. The RNA was eluted in 100 mL elution buffer and treated with DNase I (Ambion) as per the protocol. The presence of residual genomic DNA within the purified RNA was determined by real-time PCR (see below) using 200 ng of RNA as template together with the 5^0-GAPDH primer set. Samples with residual chromosomal DNA were treated again with DNase I. To retain a sufficiently high concentration of RNA after successive rounds of DNase I treatment, the samples were combined in pairs, precipitated in the presence of 1/10th volume of 5 M NaCl and two volumes of 100% ethanol, collected by centrifugation at 13,000 rpm and 48C, dried in a vacuum and resuspended in 100 ml RiboPure-Bacteria RNA elution buffer. These steps were repeated until the purified RNA was found to be free of residual chromosomal DNA.

RNA quality was visually monitored on a 1% morpholinepropanesulfonic acid–EDTA agarose gel and quantified using a NanoDrop spectrophotometer.

RNA was converted to cDNA using the 1st strand cDNA synthesis kit for RT-PCR (AMV; Roche Applied Science, Mannheim, Germany). Each cDNA synthesis reaction consisted of 750 ng of total RNA, reaction buffer added to a final 1x concentration, 5 mM $MgCl_2$, 1 mM deoxynucleotide mix, 3 mL random p(dN)6 primer, 5 U RNase inhibitor, 1.2 mL AMV reverse transcriptase and PCR grade water in a final volume of 30 mL. The reactions were incubated at 258C for 10 min followed by 428C for 60 min, 958C for 5 min, and cooling at 48C for 2 min in a thermal cycler. The cDNA was diluted 50-fold in 10 mM Tris after assessing the quality of the cDNA by real-time qPCR.

Primer Design and Real-Time Quantitative-PCR (qPCR)

Sequence-specific primer sets were designed using the LightCycler[1] Probe Design Software 2.0 (V1.0.R.36, Roche) to amplify a 140–170-bp region on the 3^0 side (where possible) of each target gene. Real-time qPCR reactions were performed in a LightCycler[1] 1.5 (Roche) using the LightCycler[1] FastStart DNA Master SYBR Green I reaction mix (Roche). The qPCR reactions were set up as per manufacturer's protocol using either 5 mL of gDNA or cDNA. Primer amplification efficiencies were determined by amplifying 10-fold serial dilutions of gDNA (purified using the Qaigen QIAamp[1] DNA Mini Kit as per manufacturer's protocol) over a range of 4–4 x 10^{-5} ng. The typical forward and reverse primer concentrations were 0.5 mM while the $MgCl_2$ concentration (2.0–3.0 mM) and primer annealing temperatures (56–678C) were optimized for each primer set (Supplementary Table SI). The amplification protocol was initiated with a 10 min pre-incubation at 958C and processed through 45 cycles of denaturation (10 s at 958C), annealing (4 s at the primer-dependant annealing temperature), and extension (7 s at 728C). The ramp rate was constant at 208C/s and the fluorescent signal was acquired at the end of each extension step. The melting curve protocol included a single cycle of denaturation for 0 s at 958C, amplicon annealing for 15 s at 108C above the primer annealing temperature and melting at a ramp rate of 0.18C/s up to 958C. The fluorescent signal was acquired continuously during the melting step. The real-time qPCR data was analysed using the Relative Expression Software Tool (REST 2009, V2.0.13) (Pfaffl et al., 2002).

Protein Sample Preparation and Two-Dimensional Electrophoresis (2DE)

A single cell pellet was resuspended in 5 mL of sterile PBS and kept on ice during sonication (two cycles of a 30 s duration with a 30 s pause). After centrifugation, the supernatant was retained on ice and the pellet was resuspended in 200 mL of CHAPS buffer (9 M urea, 4 M thiourea, and 4% w/v CHAPS) and agitated at room temperature at 200 rpm for 30 min. The insoluble fraction was removed by centrifugation and the two supernatants pooled. An equal volume of ice cold 20% w/v trichloroacetic acid solution was added and the solution kept on ice for 1 h in order to precipitate the protein. The protein was concentrated by centrifugation at 6,000 rpm for 5 min, the supernatant

removed, and the pellet subsequently washed twice with 500 mL of ice cold acetone. The washed pellet was air dried for 30 min and resuspended in 200 mL of CHAPS buffer. Protein concentrations were determined by the Bradford assay (using the Sigma–Aldrich Bradford reagent). A total of 300 mg of protein was routinely used for absorption onto a 7 cm IPG strip with either an immobilized pH 4–7 or pH 5–8 gradient (Biorad, Hercules, CA). The protein was mixed with 2 mL of ampholytes (Biorad) and 2 mL of 50% w/v DTT solution (colored with bromophenol blue). The final volume of the protein solution was made up to 125 mL and the IPG strip was passively rehydrated overnight. The rehydrated strips were subjected to isoelectric focusing using a Ettan™ IPGphor II™ (GE Healthcare, Amersham, UK) in a stepwise program for 3,500 V h at 208C. After isoelectric focusing, the strips were equilibrated in a 1% DTT solution for 20 min and then separately in a 2.5% iodoacetamide solution for 15 min. Both solutions were made up in SDS equilibration buffer (50 mM Tris–HCl buffer, 6 M urea, 0.25% DTT, 30% glycerol, and 1% SDS). The equilibrated strips were loaded onto a 12% SDS gradient gel for electrophoresis in the second dimension at 100 V. After electrophoresis the protein spots were detected by Coomassie Brilliant Blue staining and digitized with the PharosFX ™ plus molecular image scanner (Biorad). Spots that showed reproducible differences in the t-test from PD Quest ($P < 0.05$) were selected for mass spectrometry analysis. Gels were run in triplicate for each condition and for comparative analysis.

In Gel Tryptic Digestion and Matrix Assisted Laser Desorption Ionization Time of Flight Mass Spectrometry (MALDI TOF) Identification Spots of interest were excised manually, washed twice with 50 mM ammonium bicarbonate for 5 min and once more for 30 min, vortexing occasionally. The gel pieces were destained twice with 50% v/v 50 mM ammonium bicarbonate and 50% v/v acetonitrile for 30 min, vortexing occasionally, and dehydrated with 100 mL acetonitrile for 5 min. Finally, they were desiccated using the Speed Vac SC100 (ThermoSavant, Waltham, MA). Proteins were in-gel digested overnight at 378C with approximately 120 ng sequencing grade modified trypsin (Promega, Madison, WI) dissolved in 25 mM ammonium bicarbonate. Protein digestion was terminated by adding 100 mL of 1% v/v trifluoroacetic acid (TFA) and incubating for 2–4 h at room temperature before storage at 48C until further analysis.

Prior to identification, the samples were pre-treated by reverse phase chromatography using ZipTip$_{C18}$[1] (Millipore, Billerica, MA) pre-equilibrated in 100% acetonitrile, washed with 0.1% TFA, and eluted with 50% v/v acetonitrile. One microliter from each sample was mixed with the same volume of a-cyano-4-hydroxycinnamic acid (CHCA) matrix and spotted onto a MALDI target plate for analysis using a MALDI-TOF mass spectrometer. The Voyager DE Pro Biospectrometry workstation (Applied Biosystems, Forster City, CA) was used to generate a peptide mass fingerprint. All MALDI spectra were calibrated using sequazyme calibration mixture II containing angiotensin I, ACTH (1–17 clip), ACTH (18–39 clip), ACTH (7–38 clip), and bovine insulin (Applied Biosystems). The NCBI and MSDB peptide mass databases were searched using MASCOT

(http://www.matrixscience.com/search_form_select.html) with 100 ppm accuracy and oxidation as variable modification selected.

Results and Discussion

Continuous Culture Maintenance and Establishment of Steady States in Control and Microaerobic Environments

Continuous cultures of G. thermoglucosidasius NCIMB 11955 were maintained on D-glucose at a dilution rate of 0.05 h^{-1} under both aerobic and microaerobic conditions. Cultures were monitored for biomass (OD_{600}) and redox potential and supernatants were analyzed for organic acid production. The stability of these parameters (data not shown) confirmed that all cultures had attained steady state.

Two separate continuous cultures were used for the gene expression and proteome analyses. Aerobic (control) steady states were achieved at redox levels of between -22 and -31 mV, respectively, and the well-established metabolite production profiles of the organism (Cripps et al., 2009; Tang et al., 2009) showed no significant fermentative metabolism, consistent with the aerobic status. The microaerobic "switch," generated by a fivefold reduction in aeration, decreased redox potentials to between -180 and -220 mV at steady state for the two continuous cultures. The formation of organic acids (14.7–17.4 mM formate, 47.3–53.1 mM acetate, 38.6 mM ethanol, and 70.0 mM lactate) was consistent with a switch to fermentative metabolism. Ethanol and lactate were not detected in the spent media during the -180 mV low redox steady state. The corresponding genes (adhE and ldh) were, however, up-regulated (see Glycolysis Section and Supplementary Table SII) though the products may have been metabolized due to a slightly more positive redox state. Despite the difference in ethanol and lactate levels between the two low redox cultures, the high versus low redox steady state cultures were considered suitable for comparative analysis of the non-fermentative and fermentative physiological states. RNA Isolation, cDNA Synthesis, and Validation of Real-Time qPCR

RNA was extracted from cells harvested during high (-22 mV) and low (-180 mV) redox steady states, and an average concentration of 154 ± 2 and 65 ± 1 ng/mL of RNA (for the high and low redox steady state cultures, respectively) was obtained. The synthesized cDNA was found to be free of PCR inhibitors, determined by measuring the similarity in the amplification gradient (0.1477 ± 0.052) and linearity ($R^2 \geq 0.998$) across a twofold dilution series spanning five dilutions for each sample. The integrity of the cDNA was measured using an adapted 3^0:5^0 integrity assay in which the ratio of the 3^0 and 5^0 ends of a selected cDNA transcript is quantitatively compared after real-time PCR (Nolan et al., 2006). For all samples the 3^0:5^0 ratios were between 0.75:1 and 1.12:1, thus comparing well to that of the genomic DNA (1.21:1) and suggesting that the cDNA was of suitable purity and integrity for real-time qPCR analysis.

The G. thermoglucosidasius recN and trmE transcripts were chosen to normalize the cDNA samples during expression analysis. The recN gene encodes a protein involved in

recombination repair and in E. coli is strictly regulated by LexA during the SOS response (Kuzminov, 1999). The trmE gene (also referred to as thdF) encodes the GTPase enzyme TrmE, a tRNA modification enzyme involved in gene translation where, in E. coli, expression is not affected by oxygen availability (Partridge et al., 2007). No changes in the levels of recN or trmE transcripts were observed under experimental conditions (Supplementary Table SII).

2D Gel Image Generation and Comparison of Control and Microaerobic Proteomes

Cell pellets from both steady state cultures, exhibiting a 189 mV difference in redox potential (-31 to -220 mV), were lysed and the total soluble protein was characterized by 2DE. Representative gels are shown in Supplementary Figure S1. Replica gels were prepared for either condition and the gels were digitized and analyzed using PDQuest (Biorad). For each state the total number of expressed proteins was calculated and differences were quantified, based on comparative analysis of spot densities.

Statistical analysis revealed that 151 proteins were differentially regulated between both proteomes (Table I). Relative to the control, 58 proteins were down-regulated in response to a decrease in redox potential, while 85 were up-regulated. No proteins were detected that were wholly repressed but eight proteins were found to be exclusively expressed under microaerobic conditions. Variation patterns derived from each spot were analyzed statistically and found to be consistent across the triplicate gels produced for each condition.

Table I. Proteins identified as differentially regulated in *G. thermoglucosidasius* NCBI 11955 in response to a switch to a low redox environment.

Mode of regulation	Protein number	Accession number	Organism	Protein	Theoretic pI/Mwt	Practical pI/Mwt	Mowse Score	Fold change (aerobic to microaerobic; spot volume)
Exclusively expressed	2	—	—	No match found	—	—	—	—
	16, 17	Gi 171325280	*Geobacillus* sp. WCH70	Formate acetyltransferase	6.0/85	7.2/74	144, 149	—
	18, 19	Gi 255333088	*Geobacillus* sp. Y4.1MC1	NADH: Flavin oxidoreductase/NADH oxidase FAD dependent oxidoreductase			68	—
	21, 22	Gi 255330984	*Geobacillus* sp. Y4.1MC1	CrispR associated protein			70, 74	—
	20	—	—	No match found	—	—	—	—
Up-regulated	12	Gi 56421589	*G. kaustophilus* HTA426	Phosphopyruvate hydratase	4.8/46	5.2/40	75	4.2
	23	Q5LOC4_	*G. kaustophilus* HTA426	Glutamine synthetase	5.2/51	5.2/51	5.7/48	17.0
	3	Q2EIA2 BACTU	*Bacillus thuringiensis* serovar *thuringiensis*	Flagellin	5.2/36	6.5/36	62	1.6
	4	Q5KUQ8 GEOKA	*G. kaustophilus* HTA426	Hypothetical protein (peptidase)	5.3/54	6.6/35	69	1.2
	5, 25, 26, 27	Gi 171326327	*Geobacillus* sp. WCH70	Isocitrate dehydrogenase	5.5/47	5.9/42	83, 83, 86, 81	4.5
	6, 24	Gi 171325271	*Geobacillus* sp. WCH70	Alanine dehydrogenase	5.7/40	6.1/40	156, 135	17.0
	7	—	—	No match found	—	—	—	1.6
	8	Q73CF0 BACC1	*Bacillus cereus* ATCC 10987	Glyoxalase family protein	5.5/36	4.9/28	69	2.3
	9	—		No match found	—	—	—	2.2
	10	Gi 171324338	*Geobacillus* sp. WCH70	Dihydrolipoamide dehydrogenase	5.2/60	5.8/57	100	17.7
	11	—		No match found	—	—	—	1.1
	15	Q5KUJ3_GEOKA	*G. kaustophilus* HTA426	F0F1-type ATP synthase	5.0/52	5.5/50	183	1.6
	28	Gi 56421207	*G. kaustophilus* HTA426	Succinate dehydrogenase flavoprotein subunit	6.1/65	6.5/60	137	0.8
	29, 30	Gi 171326365	*Geobacillus* sp. WCH70	Inosine-5'-monophosphate dehydrogenase	5.9/53	6.7/50	184, 186	1.17
Down-regulated	1	Q5KW58 GEOKA	*G. kaustophilus* HTA426	Acetate CoA ligase	5.6/60	7.9/23	70	70.4
	13	Gi 138896930	*G. thermodenitrificans* NG80-2	NADH dehydrogenase subunit D	5.7/42	5.6/78	72	1.8
	14	Gi 171323301	*Geobacillus* sp. WCH70	Superoxide dismutase	5.6/23	6.1/18	73	11.6

Protein Excision and Identification

Protein spots demonstrating the largest degree of differential regulation (up, down and de novo expression) were chosen for MADLI-TOF analysis. A total of 30 proteins were chosen for identification, excised from the corresponding gels, and digested with trypsin. Relative peptide mass fingerprints were generated and compared to possible peptide mass profiles generated by the Mascot search engine (Matrix Science, Boston, MA). Identification confidence was based on the MOWSE values generated (MOWSE values for each protein dictate that the mass values of the peptide fingerprint fall within a given mass tolerance of an experimental value). The identity of each excised protein, together with the level of regulation, the theoretical and practical pI values and molecular weight, is shown in Table I, As might be predicted, many proteins differentially expressed in response to a decrease in redox potential are involved in glycolysis, the Krebs cycle and fermentation product synthesis. Intriguingly, others are involved in the electron transport chain, amino acid biosynthesis, and cellular redox maintenance.

Glycolysis

The microaerobic "switch" resulted in a general up-regulation of glycolysis, shown by a 2.5- and 6.4-fold increase in transcription for the 11 RT-PCR targeted genes (Fig. 1 and Supplementary Table SII) as well as 4.2-fold up-regulation of enolase as seen on the 2D gels (spot 12, Supplementary Fig. S1 and Table I). The pfkA, pgk, and pykF genes, encoding the three rate-limiting glycolytic enzymes phosphofructokinase, phosphoglycerate kinase, and pyruvate kinase, were up-regulated by 3.5-, 5.0-, and 4.1-fold, respectively. These changes clearly reflect increased ATP synthesis through substrate-level phosphorylation and the increased production of precursors for biomass synthesis (Jouhten et al., 2008; Peng and Shimizu, 2003; Yu et al., 2011).

Significant increases in transcription (4.1- and 2.8-fold) were observed for the phosphotransacetylase and acetate kinase-encoding genes, pta and ackA (Fig. 1). These enzymes are responsible for the conversion of acetyl-CoA to acetyl phosphate to acetate, with the synthesis of ATP from AMP. Apart from the production of ATP in response to reduced TCA cycle function, the ratio of acetate to acetyl-CoA represents an important signaling node within cells, determining the balance within central metabolism between biomass synthesis, redox balance, and energy yield (Castañ o-Cerezo et al., 2009). The acs gene and its protein product acetate-CoA ligase (or synthase), responsible for the recycling of acetate back to acetyl-CoA, was down-regulated by 20-fold at the transcriptional (Fig. 1 and Supplementary Table SII) and 70.4-fold at the translational level (spot 1; Supplementary Fig. S1 and Table I). The results, therefore, suggest that the accumulation of acetate of up to 53 mM in the spent media likely resulted from the combined effects of up regulation of acetate production and down-regulation in its recycling to acetyl-CoA.

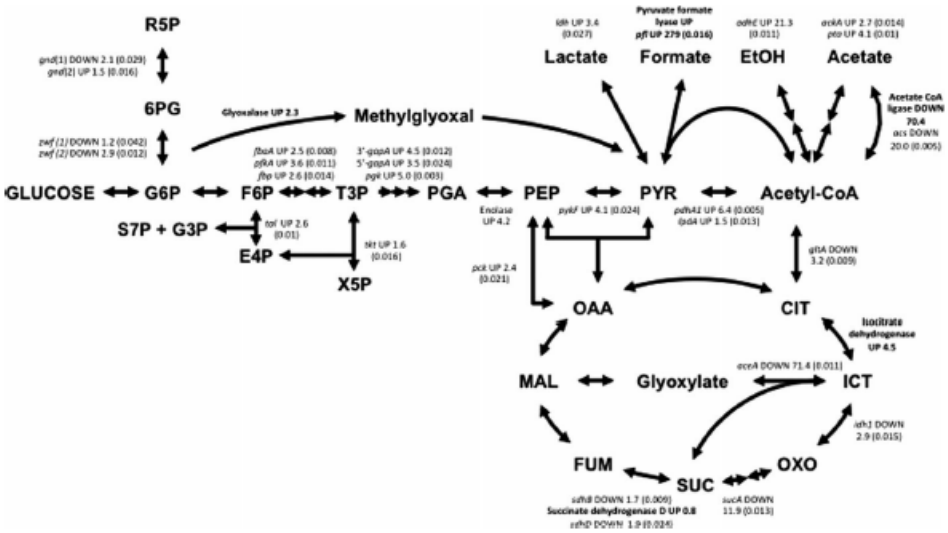

Figure 1. Gene expression and protein production ratios of *G. thermoglucosidasius* NCIMB 11955 grown under microaerobic conditions relative to an aerobic control. Only the selected transcriptional targets and proteins (identified by two-dimensional electrophoresis are indicated) relevant to glycolysis and the Krebs cycle are indicated. Gene expression and protein production ratios are given as a fold change (except for pyruvate formate lyase which was exclusively present during low redox conditions). The P(H1) values (95% confidence interval) are given in brackets. The standard deviation, standard error, and protein product for each gene target is given in Supplementary Table SII. 6PG, 6-phosphogluconate; acetyl-CoA, acetyl-coenzyme A; CIT, citrate; E4P, erythrose-4-phosphate; EtOH, ethanol; F6P, fructose-6-phosphate; FUM, fumerate; G3P, glyceraldehyde-3-phosphate; G6P, glucose-6-phosphate; ICT, isocitrate; MAL, malate; OAA, oxaloacetate; OXO, 2-oxoglutarate; PEP, phospho*enol*pyruvate; PGA, 3-phosphoglycerate; PYR, pyruvate; R5P, ribulose-5-phosphate; S7P, sedoheptulose-7-phosphate; SUC, succinate; T3P, triose-3-phosphate; X5P, xylose-5-phosphate.

The pfl gene was strongly up-regulated (279-fold: Fig. 1 and Supplementary Table SII) and its cognate protein, the pyruvate formate lyase (Pfl) was found to be exclusively present under microaerobic conditions (spot 16, 17; Supplementary Fig. S1 and Table I). Up-regulation of pfl under these conditions has been observed previously (Tang et al., 2008). Pfl is commonly associated with mediating acetyl CoA production for organic acid and alcohol synthesis (fermentation), principally because its function is severely inhibited by oxygen (Knappe and Sawers, 1990; Trotter et al., 2011). In the experimental strain used in this study, the genomic disruption of pfl has been shown to eliminate formate production (Cripps et al., 2009). We conclude, from this study and the published models, that Pfl plays a role in mediating acetyl CoA production from pyruvate, both for organic acid production and for entry into a partly functional Krebs cycle in support of an oxygen scavenging electron transport chain. Such observations have previously been presented for E. coli models under similar growth conditions (Trotter et al., 2011).

Interestingly, a glyoxalase protein was identified in aerobically grown cells and was up-regulated under microaerobic conditions. The methylglyoxal shunt can act either as a bypass for glycolysis to avoid unstable decoupling of phosphorylated glycolytic intermediate processing, or as a recovery mechanism to remove toxic methylglyoxal arising from glycolysis (Ferguson et al., 1998). Under semi-fermentative and high glycolytic flux conditions, such as are expected under microaerobic conditions and shown in this study (spots 12 and 16, 17; Supplementary Fig. S1 and Table I), methylglyoxal may be produced in high titers. The identification of an active bypass mechanism would explain reports of residual lactate production in ldh inactivation mutants of G. thermoglucosidasius (Cripps et al., 2009).

Krebs Cycle

Regulation of the Krebs cycle genes under microaerobic conditions was less uniform than for glycolysis. The gltA gene, encoding citrate synthase which catalyzes the entry of acetyl-CoA into the Krebs cycle, was down-regulated by 3.4-fold (Fig. 1). The idh1 gene, encoding isocitrate dehydrogenase, was down-regulated by only 2.9-fold at the transcriptional level (Fig. 1 and Supplementary Table SII) but was up-regulated by 4.5-fold at the protein level (Table I). A strong 11.9-fold down-regulation was observed for the alpha-ketoglutarate dehydrogenase encoding gene, sucA, which represents the second decarboxylation step in the Krebs cycle. Isocitrate can also enter the glyoxylate bypass, a pathway that allows for the cycling of carbon (derived from acetyl-CoA) within the Krebs cycle without a net loss of carbon (CO_2) through the catalytic activity of the isocitrate lyase, thereby permitting growth on acetate (Shinar et al., 2009). Expression of the aceA gene encoding the isocitrate lyase was, however, found to be down-regulated by 71.4-fold (Fig. 1), suggesting that under microaerobic conditions the glyoxylate bypass was strongly down-regulated. This is consistent with the strong down-regulation of the acs gene and its acetyl-CoA ligase product and probably also contributes to the accumulation of acetate.

Under microaerobic conditions there was little change (1.7- and 1.9-fold down-regulation) at the transcriptional level of the sdhB and sdhD genes, encoding the iron–sulfur protein and flavoprotein subunits, respectively, of the succinate dehydrogenase enzyme complex (Fig. 1). A protein tentatively identified as succinate dehydrogenase D (spot 28; Supplementary Fig. S1 and Table I) was, however, found to be slightly up-regulated (0.8-fold). The reason for a difference in the small but apparent regulation of the idh1, sdhB, and sdhD genes and the isocitrate dehydrogenase and succinate dehydrogenase proteins at the RNA and protein levels is unknown. There are no paralogs of these genes within the genome of G. thermoglucosidasius NCIMB 11955. Thus it is unlikely that pseudogenes were targeted during gene expression analyses. The possibility exists that the apparent difference in protein concentration under the two conditions may be the result of post-translational modification, which is an additional layer of regulation (Borthwick et al., 1984; Zhang et al., 2009).

Pentose Phosphate Pathway

The oxidative phase of the pentose phosphate pathway (PPP) is important for the regeneration of NADPH and the synthesis of ribose-5-phosphate, required for reductive biosynthesis and the synthesis of ribonucleotides and fatty acids (Samland and Sprenger, 2009). Glucose-6-phosphate enters the PPP and is converted to ribulose-5-phosphate by glucose-6-phosphate dehydrogenase and 6-phosphogluconate dehydrogenase, respectively. The G. thermoglucosidasius 11955 genome (NCBI accession number CP002835) contains two glucose-6-phosphate dehydrogenase-encoding genes, znf1 and znf2, and two 6-phosphogluconate dehydrogenase-encoding genes, gndA and gndB. Both pairs of genes showed little change in expression levels under microaerobic conditions (<2-fold and <3-fold down-regulation, respectively; Fig. 1). Gene expression within the non-oxidative sections of the PPP and purine metabolism also showed little change between the two redox states. Although only a

limited number of genes were targeted, the gene expression results and the failure to identify any alternate proteins suggested that overall flux within the PPP was not significantly affected by a decrease in oxygen availability or redox potential.

ATP Synthesis and the Electron Transport Chain

Several proteins were identified as significantly regulated in response to the microaerobic "switch," two of which were oxidoreductases (spots 13 and 14; Supplementary Fig. S1 and Table I). Spot 13 (down-regulated) was identified as NADH dehydrogenase subunit D, which forms part of the multienzyme NADH dehydrogenase complex. A reduction in expression of NADH dehydrogenase would be expected under fermentative conditions, consistent with a physiological shift to fermentation and away from oxidative phosphorylation. However, the up-regulation of an NADH:FAD oxidoreductase (spot 18, 19; Supplementary Fig. S1 and Table I), succinate dehydrogenase (spot 28; Supplementary Fig. S1 and Table I) and subunits of ATP synthetase (spot 15; Supplementary Fig. S1 and Table I) perhaps indicate that a modified version of the electron transport chain was still active under low redox conditions.

Spot 14 (Supplementary Fig. S1) was identified as superoxide dismutase, an iron or manganese dependent enzyme which catalyses the dismutation of superoxide and reactive oxygen species (ROS) to oxygen and hydrogen peroxide (Abreu and Cabelli, 2010). Reactive oxygen species are cytotoxic and superoxide dismutase is one of the mechanisms of protection against oxidation damage. The down-regulation of this enzyme under conditions of reduced oxygen tension (and presumably reduced ROS formation) was, therefore, not unexpected.

Summary

G. thermoglucosidasius NCIMB 11955 is a potentially valuable model for understanding physiology of thermophilic prokaryotes and may be successfully developed as an industrial tool for ethanologenesis (Cripps et al., 2009). As such, it is important to understand the fundamental metabolic (and genetic) responses to the imposition of a stressed environment, such as a low redox state and growth in a minimal media with fermentative sugar supplementation. Using a combination of targeted (transcriptomic) and non-specific (proteomic) analyses of changes in gene expression, we have demonstrated a range of responses which, taken together, are consistent with a physiological model aimed at maximizing NADH turnover and ATP synthesis under low oxygen availability. These typical O_2- deficit stress responses were supplemented with unexpected shifts in physiology such as the up-regulation of the methylglyoxal shunt. This could serve as protection against toxic phosphorylated glycolytic intermediates, which otherwise might accumulate as a result of up-regulation of glycolysis with concurrent down-regulation of the TCA cycle, as was observed for G. thermoglucosidasius NCIMB11955 during low redox conditions.

The authors wish to acknowledge the University of the Western Cape and the National Research Foundation (South Africa) for funding.

References

Abreu I, Cabelli DE. 2010. Superoxide dismutases—A review of the metal-associated mechanistic variations. Biochim Biophys Acta Proteins Proteom 1804:263–274.

Borthwick AC, Holms WH, Nimmo HG. 1984. Isolation of active and inactive forms of isocitrate dehydrogenase from Escherichia coli ML308. Eur J Biochem 141:393–400.

Castañ o-Cerezo S, Pastor J, Renilla S, Bernal V, Iborra J, Cá novas M. 2009. An insight into the role of phosphotransacetylase (pta) and the acetate/ acetyl-CoA node in Escherichia coli. Microb Cell Fact 8:54.

Clomburg JM, Gonzalez R. 2010. Biofuel production in Escherichia coli: The role of metabolic engineering and synthetic biology. Appl Microbiol Biotechnol 86(2):419–434.

Cripps RE, Eley K, Leak DJ, Rudd B, Taylor M, Todd M, Boakes S, Martin S, Atkinson T. 2009. Metabolic engineering of Geobacillus thermoglucosidasius for high yield ethanol production. Metab Eng 11:398–408.

Ferguson GP, Tö temeyer S, MacLean MJ, Booth IR. 1998. Methylglyoxal production in bacteria: Suicide or survival? Arch Microbiol 170(4): 209–218.

Hahn-Hagerdal B, Galbe M, Gorwa-Grauslund MF, Liden G, Zacchi G. 2006. Bio-ethanol—The fuel of tomorrow from the residues of today. Trends Biotechnol 24(12):549–556.

Jouhten P, Rintala E, Huuskonen A, Tamminen A, Toivari M, Wiebe M, Ruohonen L, Penttilä M, Maaheimo H. 2008. Oxygen dependence of metabolic fluxes and energy generation of Saccharomyces cerevisiae CEN. PK113-1A. BMC Syst Biol 2:60–79.

Knappe J, Sawers G. 1990. A radical-chemical route to acetyl-CoA: The anaerobically induced pyruvate formate-lyase system of Escherichia coli. FEMS Microbiol Rev 75(4):383–398.

Kuzminov A. 1999. Recombinational repair of DNA damage in Escherichia coli and bacteriophage lambda. Microbiol Mol Biol Rev 63(4):751–813. Matsushika A, Inoue H, Kodaki T, Sawayama S. 2009. Ethanol production from xylose in engineered Saccharomyces cerevisiae strains: Current state and perspectives. Appl Microbiol Biotechnol 84(1):37–53.

Nolan R, Hands RE, Bustin SA. 2006. Quantification of mRNA using real-time RT-PCR. Nature Protocols 1(3):1559–1582.

Panesar PS, Marwaha SS, Kennedy JF. 2006. Zymomonas mobilis: An alternative ethanol producer. J Chem Technol Biotechnol 81(4): 623–635.

Partridge JD, Sanguinetti G, Dibden DP, Roberts RE, Poole RK, Green J. 2007. Transition of Escherichia coli from aerobic to micro-aerobic conditions involves fast and slow reacting regulatory components. J Biol Chem 282:11230–11237.

Patnaik R. 2008. Engineering complex phenotypes in industrial strains. Biotechnol Prog 24(1):38–47.

Peng L, Shimizu K. 2003. Global metabolic regulation analysis for Escherichia coli K12 based on protein expression by 2-dimensional electrophoresis and enzyme activity measurement. Appl Microbiol Biotechnol 61(2):163–178.

Pfaffl MW, Horgan GW, Dempfle L. 2002. Relative expression software tool (REST) for group-wise comparison and statistical analysis of relative expression results in real-time PCR. Nucleic Acids Res 30(9):e36.

Rogers PL, Jeon YJ, Lee KJ, Lawford HG. 2007. Zymomonas mobilis for fuel ethanol and higher value products. Adv Biochem Eng Biotechnol 108:263–288.

Samland AK, Sprenger GA. 2009. Transaldolase: From biochemistry to human disease. Int J Biochem Cell Biol 41(7):1482–1494.

Shaw AJ, Podkaminer KK, Desai SG, Bardsley JS, Rogers SR, Thorne PG, Hogsett DA, Lynd LR. 2008. Metabolic engineering of a thermophilic bacterium to produce ethanol at high yield. Proc Natl Acad Sci USA 105(37):13769–13774.

Shinar G, Rabinowitz JD, Alon U. 2009. Robustness in glyoxylate bypass regulation. PLoS Comput Biol 5(3):e1000297.

Tang YJ, Sapra R, Joyner D, Hazen TC, Myers S, Reichmuth D, Blanch H, Keasling JD. 2009. Analysis of metabolic pathways and fluxes in a newly discovered thermophilic and ethanol-tolerant Geobacillus strain. Biotechnol Bioeng 102(5):1377–1386.

Taylor MP, Eley KL, Martin S, Tuffin MI, Burton SG, Cowan DA. 2009. Thermophilic ethanologenesis: Future prospects for second-generation bioethanol production. Trends Biotechnol 27(7):398–405.

Trotter EW, Rolfe MD, Hounslow AM, Craven CJ, Williamson MP, Sanguinetti G, Poole RK, Green J. 2011. Reprogramming of Escherichia coli K-12 metabolism during the initial phase of transition from an anaerobic to a micro-aerobic environment. PLoS ONE 6(9): e25501.

Wang Z, Chen M, Xu Y, Li S, Lu W, Ping S, Zhang W, Lin M. 2008. An ethanol-tolerant recombinant Escherichia coli expressing Zymomonas mobilis pdc and adhB genes for enhanced ethanol production from xylose. Biotechnol Lett 30(4):657–663.

Yu W, Gao S, Yin C, Zhou Y, Ye B. 2011. Comparative transcriptome analysis of Bacillus subtilis responding to dissolved oxygen in adenosine fermentation. PLoS ONE 6(5):e20092.

Zhang J, Sprung R, Pei J, Tan X, Kim S, Zhu H, Liu CF, Grishin NV, Zhao Y. 2009. Lysine acetylation is a highly abundant and evolutionarily conserved modification in Escherichia coli. Mol Cell Proteomics 8(2):215–225.

Zhou B, Martin GJ, Pamment NB. 2008. Increased phenotypic stability and ethanol tolerance of recombinant Escherichia coli KO11 when immobilized in continuous fluidized bed culture. Biotechnol Bioeng 100(4):627–633.